

# A consistent analysis of three years of ground- and space-based photometry of TrES-2

S. Schröter, J.H.M.M. Schmitt, and H.M. Müller

Hamburger Sternwarte, Universität Hamburg, Gojenbergsweg 112, 21029 Hamburg, Germany  
e-mail: ssschroeter@hs.uni-hamburg.de

Received November 29, 2011; accepted January 26, 2012

## ABSTRACT

The G0V dwarf TrES-2A, which is transited by a hot Jupiter, is one of the main short-cadence targets of the *Kepler* telescope and, therefore, among the photometrically best-studied planetary systems known today. Given the near-grazing geometry of the planetary orbit, TrES-2 offers an outstanding opportunity to search for changes in its orbital geometry. Our study focuses on the secular change in orbital inclination reported in previous studies. We present a joint analysis of the first four quarters of *Kepler* photometry together with the publicly available ground-based data obtained since the discovery of TrES-2b in 2006. We use a common approach based on the latest information regarding the visual companion of TrES-2A and stellar limb darkening to further refine the orbital parameters. We find that the *Kepler* observations rule out a secular inclination change of previously claimed order as well as variations of the transit timing, however, they also show slight indication for further variability in the inclination which remains marginally significant.

**Key words.** stars: individual: TrES-2 - stars: planetary systems

## 1. Introduction

The transiting Jovian planet TrES-2b was originally discovered by O'Donovan et al. (2006), and later extensively observed by Holman et al. (2007) and Sozzetti et al. (2007), who determined more accurate properties for the TrES-2 system. TrES-2A is an old ( $\approx 5$  Gyr) G0V star with about solar radius and mass, orbited by a close-in (0.035 AU) planet with a mass of  $1.2 M_J$  and a period of 2.47 d. The planet has a radius of  $1.24 R_J$  and a large inclination angle of about  $84^\circ$ , implying a nearly grazing transit. The spectroscopic parameters of the system determined by Sozzetti et al. (2007) were confirmed and refined by Ammler-von Eiff et al. (2009).

As already pointed out by Holman et al. (2007), TrES-2 offers an outstanding opportunity to search for changes in orbital parameters for several reasons: Its large inclination and close-in orbit yield a high impact parameter, making the shape and timing of the transit sensitive to variations of the orbital parameters. Its large radius and short orbital period allow the study of large numbers of deep transits over hundreds of epochs. Additionally, TrES-2 is in the field of view of the *Kepler* telescope, which has already gathered more than 220 days of publicly available photometric data, probably making TrES-2 the photometrically best-studied exoplanetary system to date.

Since its discovery there have been numerous attempts to detect secular changes in the orbital parameters of TrES-2b due to an external perturber. Mislis & Schmitt (2009) combined their own transit observations with the data from Holman et al. (2007) and found these data to be consistent with a decrease in transit duration, suggesting a decrease of about  $0.075^\circ/\text{yr}$  in the orbital inclination of the planet, an interpretation corroborated by another series of observations (Mislis et al. 2010). Reverting to secular perturbation theory, Mislis et al. (2010) suggest that a Jovian mass planet with a period between 50 to 100 days can explain the observed inclination changes. On the other hand, Scuderi et al. (2010), in their analysis from data taken in June 2009, find sys-

tematically higher values for the inclination of TrES-2b, ruling out any systematic trend. Their analysis also includes 33 days of *Kepler* data comprising multiple transits originally published by Gilliland et al. (2010), which they find to be in agreement with their ground-based observations.

Additional photometric data of TrES-2 are presented by Rabus et al. (2009), who analyze five transits systematically searching for signatures of transit timing variations. However, they do not find a clear signal and are only able to provide upper constraints on the perturber's mass. Christiansen et al. (2011) obtained nine additional transits from NASA's EPOXI Mission of Opportunity (Deep impact). Comparing their results with earlier measurements, they find a formally significant decrease in the transit duration with time, which however disappears if they exclude the duration measurement by Holman et al. (2007).

A thorough analysis of the first two quarters of *Kepler* data (Q0 and Q1) is presented by Kipping & Bakos (2011b), who do not find any inclination change within the *Kepler* data, obtaining an inclination change of  $(+0.0019 \pm 0.0020)^\circ/\text{cycle}$ . They also reanalyze the data by Holman et al. (2007) fitting the limb-darkening coefficients and compare the measured average transit durations in both data sets. Their results neither support nor exclude the inclination change, largely due to the still very small temporal baseline of 18 cycles. Raetz et al. (2009, 2011) analyze 22 additional transits observed between March 2007 and August 2010, but find no indications of variations in the transit duration. However, their data quality does not suffice to exclude the inclination change proposed by Mislis et al. (2010).

The whole discussion is further complicated by the results of Daemgen et al. (2009), who detected a visual companion to TrES-2A at a separation of  $1.089 \pm 0.008''$  that contaminates the photometric data, and leads to filter-dependent deviations in the orbital parameters if not being accounted for. While Scuderi et al. (2010) already mention the contribution of a third light and estimate its influence on the system parameters, Kipping &

Bakos (2011b) were actually the first to include it in their light-curve modeling of the *Kepler* data.

The purpose of this work is to present a joint analysis of all publicly available *Kepler* data of TrES-2 focussing on the apparent change in orbital inclination as proposed by Mislis et al. (2010). We exploit four quarters of *Kepler* photometry and publicly available ground-based transit observations in a joint approach including the latest observational results regarding the TrES-2-system, aiming at a consistent picture of the observational status quo regarding changes in the orbital parameters, especially the inclination of the planet.

## 2. Light-curve modeling

We fit the transit data with the transit model developed by Mandel & Agol (2002) making use of their occultquad and occultnl FORTRAN routines<sup>1</sup>. From the transit light curve, we can directly infer the following parameters: the orbital period,  $P$ , the time of transit minimum,  $\tau$ , the radius ratio,  $p = R_p/R_s$ , the semi-major axis in stellar radii,  $a/R_s$ , the orbital inclination,  $i$ , and the limb-darkening law. For our fits we either assume a quadratic limb darkening with coefficients  $u_1$  and  $u_2$  or a four-parametric non-linear prescription as proposed by Claret & Bloemen (2011, their Eq. 5), which provides a significantly more accurate representation of model atmosphere intensities (Howarth 2011a). Furthermore, our model includes the contribution of a third light,  $L_3$ , given as a fraction of the host-star's luminosity.

We assume a circular orbit fixing  $e = 0$ , as there are no indications for any non-zero eccentricity (Kipping & Bakos 2011b).

### 2.1. On the role of limb darkening

There is an ongoing debate on the role of limb darkening in the analysis of planetary transit light curves regarding the question whether the limb-darkening coefficients (LDCs) should be fitted together with the remaining parameters or left fixed during the fit. On the one hand, LDCs are the only quantities in the parameter set describing the transit that can be predicted theoretically, given some basic spectroscopic information of the object. As such they are inherently dependent on the quality of available spectroscopic data and the subtleties of underlying assumptions entering the model calculations itself. Fitting the LDCs therefore assures that the resulting transit parameters are independent of the spectroscopic background model and that the uncertainties of the spectroscopic parameters are readily included into the transit model. Furthermore, the inclusion of LDCs as free parameters in the fitting process leads to considerably larger uncertainties in the remaining model parameters, reflecting the fact, that the LDCs are highly correlated to most parameters.

On the other hand, the data quality of most ground-based measurements is not sufficient to substantially constrain the LDCs. Several fit parameters, especially the LDCs, are known to be mutually correlated, as demonstrated analytically by Pál (2008) and numerically by Southworth (2008) in the specific case of TrES-2. The mutual correlations among the parameters are particularly strong in the case of TrES-2, where the transit is nearly grazing, because TrES-2b only covers the outermost parts of the stellar disk that are dominated by strong limb-darkening effects. The remaining orbital parameters thus depend crucially on the details of the adopted limb darkening resulting in strong correlations with the LDCs. The amount of information on the limb darkening, which can be extracted even from the *Kepler*

**Table 1.** Spectroscopic parameters of TrES-2

	Sozzetti et al. (2007)	Ammler-von Eiff et al. (2009)
$T_{\text{eff}}$ (K)	$5850 \pm 50$	$5795 \pm 73$
$\log g$ (cgs)	$4.4 \pm 0.1$	$4.30 \pm 0.13$
$\xi_T$ (km/s)	$1.00 \pm 0.05$	$0.79 \pm 0.12$
[M/H]	$-0.15 \pm 0.10$	$0.06 \pm 0.08$

data, is limited by the fact, that the transit of TrES-2b is nearly grazing, i.e.  $\mu \ll 1$ . Assuming a quadratic limb-darkening law this approximation yields

$$\frac{I(\mu)}{I_0} = 1 - (u_1 + u_2) + \mu(u_1 + 2u_2) - O(\mu^2). \quad (1)$$

Therefore, to zeroth order we are only sensitive to the sum of the LDCs, i.e. the amount of deducible knowledge on the individual parameter is inherently limited. This introduces a degeneracy between both LDCs due to their strong correlation. While, in principle, it would always be preferable to fit for LDCs, thereby cross-checking spectroscopic results and theoretical modeling, analyses of ground-based observations of TrES-2 cannot afford to refrain from including as much independently obtained information as possible.

Therefore, in a first attempt, we will fit the *Kepler* data without assuming any a priori information on the LDCs (see Sect. 4.1) and compare our results to theoretical predictions. However, comparing the results from the *Kepler* data to several ground-based transit observations requires a common treatment of the data. We therefore eventually use fixed LDCs for all data sets assuming the theoretically predicted values (see Sect 4.2).

The spectroscopic studies by Sozzetti et al. (2007) and Ammler-von Eiff et al. (2009) concordantly suggest that TrES-2A has an effective temperature of 5800 K, a surface gravity of 4.4, microturbulence velocity of 1 km/s and solar metallicity (see Table 1). Claret & Bloemen (2011) provide LDCs in several filter bands calculated for a grid of PHOENIX and ATLAS9 model atmospheres, employing two different calculation methods. We linearly interpolated on the data grid to obtain a set of LDCs pertaining to a PHOENIX model closely matching the inferred spectroscopic properties of TrES-2A. Our interpolated LDCs for the different filter bands are summarized in Table 2.

### 2.2. On the contribution of a third light

Daemgen et al. (2009) report the detection of a faint visual companion of TrES-2A in their ground-based high-resolution images obtained with the *AstraLux* lucky imaging camera at Calar Alto. The angular distance from TrES-2A to this object is only  $1.089 \pm 0.009''$ . It contaminates all previous published observations and introduces a systematic error in the transit parameters, especially the transit depth. According to Southworth (2010), roughly 5% of third light can be compensated for by decreasing  $a/R_s$  by 1%,  $p$  by 3% and  $i$  by 0.1 degrees.

Daemgen et al. (2009) measured magnitude differences in the Sloan Digital Sky Survey (SDSS)  $z'$  and  $i'$  filters, that can be used to obtain the flux contribution of the third light,  $L_3$ . They find  $\Delta z' = 3.429 \pm 0.010$  and  $\Delta i' = 3.661 \pm 0.016$  resulting in flux contributions of  $0.0425 \pm 0.0004$  and  $0.0343 \pm 0.0005$  in the  $z'$  and  $i'$  bands, respectively. We assume that the nearby companion has an effective temperature of 4400 K, surface gravity of 4.5, solar metallicity and microturbulent velocity of 2 km/s compatible with its spectral type being K4.5 to K6 as derived by Daemgen et al. (2009). We used Gray's SPECTRUM together

<sup>1</sup> <http://www.astro.washington.edu/users/agol>

**Table 2.** Non-linear limb-darkening coefficients obtained by linear interpolation on the tables provided by Claret & Bloemen (2011) based on PHOENIX atmosphere models. The last column gives the fraction of flux due to the visual companion detected by Daemgen et al. (2009).

Filter	$a_1$	$a_2$	$a_3$	$a_4$	$L_3$
<i>Kepler</i>	0.473 <sup>a</sup>	0.192 <sup>a</sup>	-	-	0.0276
<i>Kepler</i>	0.801	-0.676	1.053	-0.388	0.0276
Strömgren u	0.910	-1.006	1.388	-0.355	0.0045
Strömgren v	0.863	-0.767	1.872	-0.617	0.0102
Strömgren b	0.698	-1.206	1.572	-0.599	0.0180
Strömgren y	0.758	-0.663	1.203	-0.454	0.0227
Johnson U	1.085	-1.412	1.721	-0.466	0.0053
Johnson B	0.754	-0.937	1.734	-0.641	0.0137
Johnson V	0.742	-0.602	1.134	-0.434	0.0216
Cousins R	0.796	-0.632	0.993	-0.378	0.0294
Cousins I	0.853	-0.746	0.963	-0.363	0.0360
SDSS i'	0.829	-0.688	0.935	-0.354	0.0343 <sup>b</sup>
SDSS z'	0.861	-0.807	0.967	-0.360	0.0425 <sup>b</sup>

**Notes.** <sup>(a)</sup> Interpolated coefficients for a quadratic limb-darkening law. <sup>(b)</sup> Values are based on magnitude differences directly measured by Daemgen et al. (2009).

with a Kurucz atmosphere model to calculate a synthetic spectrum. We then use STScI's *pysynphot*<sup>2</sup> to convolve the spectrum with transmission curves of all standard filter systems, taking into account the high-resolution *Kepler* response function<sup>3</sup> to obtain the throughput in *Kepler*'s broad spectral band. The resulting fractional contributions of third light,  $L_3$ , are tabulated in Table 2.

### 2.3. Fitting approach and error analysis

To obtain adequate errors for the fit parameters and to determine the mutual dependence of the parameters, we explore the parameter space by sampling from the posterior probability distribution using a Markov-Chain Monte-Carlo (MCMC) approach.

Typically, the system parameters, especially the LDCs, are prone to substantial correlation effects. These correlations can easily render the sampling process inefficient. It is therefore advisable to use a suitably decorrelated set of LDCs as e.g. proposed by Pál (2008). However, due to the near-grazing system geometry in the case of TrES-2 we expect strong correlations between the whole set of parameters. We therefore chose to use a modification of the usual Metropolis-Hastings sampling algorithm, which is able to adapt to the strong correlation structure. This modification, known as Adaptive Metropolis algorithm (AM; Haario et al. 2001), releases the strict Markov property of the sampling chains by updating the sampling parameters using a multivariate jump distribution whose covariance is tuned during sampling. This tuning is based on all previous samples of the chain, so that AM loses the Markov property. However, the algorithm can be shown to have the correct ergodic properties, i.e. it approaches the correct posterior probability distribution under very general assumptions (Haario et al. 2001; Vihola 2011). We checked that AM yields correct results for simulated data sets with parameters close to TrES-2, and found that this approach showed fast convergence and efficiency.

All MCMC calculations make extensive use of routines of PyAstronomy<sup>4</sup>, a collection of Python routines providing a convenient interface to fitting and sampling algorithms implemented in the PyMC (Patil et al. 2010) and SciPy (Jones et al. 2001) packages.

### 3. Data preparation

We retrieved the *Kepler* data of quarters Q0 to Q3 from the NASA Multimission Archive at STScI<sup>5</sup>. Specifically, we use data pertaining to data release 5 (Q0, Q1), data release 7 (Q2), and data release 4 (Q3) as provided by the *Kepler* Data Analysis Working Group<sup>6</sup>. *Kepler* observed TrES-2 in short cadence mode with a sampling of 58.85 s covering 229 days. For our analysis, we use the raw aperture photometry (SAP) flux and the corresponding error as provided in the FITS files. The raw data have been processed using *Kepler*'s Photometric Analysis (PA) pipeline, which includes barycentric time correction, detection of Argabrightening (a transient increase of background flux possibly due to dust particles) and cosmic ray events, background removal, and the computation of aperture corrected flux. Further, we removed invalid data points and all points marked by the SAP-QUALITY flag. The *Kepler* data provide time stamps in Barycentric Julian Dates (BJD<sub>UTC</sub>), which we convert into Barycentric Dynamical Time (BJD<sub>TDB</sub>) accounting for 34 leap seconds elapsed since 1961.

The data show discontinuities and exponential jumps due to instrumental duty cycles (“pointing tweaks”, “safe mode recoveries”, and “earth points”) and long-term trends (“focus drifts”), which must be corrected beforehand. First, we removed all transits from the light curve including one half of the transit duration on either side and rejected  $3\sigma$  outliers using a sliding median filter of window size 30 minutes. We then used the information provided in the data release notes to exclude data points affected by safe mode recoveries and earth points, which are difficult to correct otherwise. Subsequently, we divided the data into chunks covering undisturbed duty cycles. As there are two pointing tweaks occurring during quarter Q2, we subdivided the Q2 data at these tweaks into three chunks covering full duty cycles.

To remove long-term trends due to focus drifts, we followed an approach similar to Kipping & Bakos (2011b) by using the discrete cosine transform (Makhoul 1980) to obtain a smoothed model of the continuum for each data chunk separately. The discrete cosine transform decomposes a signal  $x(n)$  into a linear combination of  $N$  cosine functions according to

$$y(k) = \sum_{n=0}^{N-1} x(n) \cos\left(\frac{\pi k(2n+1)}{2N}\right), \quad 0 \leq k < N, \quad (2)$$

and provides an efficient way of extracting the low-frequency information within the signal. We applied the discrete cosine transform to each chunk of the light curve removing all but the first  $l$  low-frequency terms, where  $l$  is the rounded integer value of the length of the chunk divided by the orbital period. The thus cleaned transformed signal was inversely transformed to obtain a smoothed model of the continuum. Finally, we divided the complete light curve including the transits by the model and extracted the data in a box of half-width 0.06 days around

<sup>4</sup> <http://www.hs.uni-hamburg.de/DE/Ins/Per/Czesla/PyA/PyA/index.html>

<sup>5</sup> <http://archive.stsci.edu/kepler/>

<sup>6</sup> [http://archive.stsci.edu/kepler/release\\_notes](http://archive.stsci.edu/kepler/release_notes)

<sup>2</sup> <http://stdas.stsci.edu/pysynphot/>

<sup>3</sup> <http://keplergo.arc.nasa.gov/CalibrationResponse.shtml>

**Table 3.** Publicly available data of ground-based photometric observations of TrES-2. The epoch refers to the first transit of TrES-2b observed by O’Donovan et al. (2006).

Epoch	Filter	Reference
13, 15, 34	z’	Holman et al. (2007)
263	near R	Mislis & Schmitt (2009)
312	I	Mislis & Schmitt (2009)
395	I	Mislis et al. (2010)
414	I,y,b,v	Mislis et al. (2010)
421	I	Scuderi et al. (2010)

each transit center. We further discard three transits, which occur close to the pointing tweaks, where the continuum flux shows strong distortions.

To check that the results of our study do not depend on the details of the data reduction, we also extracted the un-detrended data directly around each transit center and divided the transit by a third-order polynomial fit to the local continuum (Welsh et al. 2010). We find, that this procedure yields essentially the same results.

The ground-based data covering a total of 8 planetary transits between 2006 and 2009 are used as provided by the authors (see Table 3, for references). The time stamps are specified as Heliocentric Julian Dates ( $HJD_{UTC}$ ) and are converted into  $BJD_{TDB}$  using the webtool by Eastman et al. (2010).

#### 4. Fitting results

Before fitting the *Kepler* data, we use all available data to obtain estimates of the period,  $P$ , and the time of transit minimum,  $\tau$ . As already pointed out by Southworth (2008),  $P$  and  $\tau$  are usually correlated with each other, but uncorrelated with the remaining parameters. Therefore, the period can be determined quite accurately without interference of other parameters. Fitting all publicly available data we obtained

$$\tau_0 = 2453957.635486^{+0.000069}_{-0.000068} \text{ BJD}_{TDB} \text{ and}$$

$$P = 2.470613402^{+0.000000150}_{-0.000000154} \text{ d,}$$

where  $\tau_0$  refers to the first transit of TrES-2b observed by O’Donovan et al. (2006) and errors correspond to 68.3 % HPD (highest probability density) intervals. The fractional error in  $P$  is approximately  $10^5$  times smaller than the fractional errors in  $a/R_s$  and  $p$ , and can safely be ignored. We checked that including both parameters with Gaussian priors corresponding to their errors in the MCMC calculations yields negligible changes in the remaining parameters but slows down the MCMC algorithm. In the following, we therefore fix these parameters to their best-fit values.

##### 4.1. Four quarters of Kepler data

In the following, we fit all 81 transits observed by *Kepler* during the first four quarters of observations. To explore the whole parameter space of solutions, we relax the constraints on the parameters as much as possible by imposing uniform prior probability distributions allowing large parameter variations. By fixing the LDCs to their theoretically computed values we would impose strong a priori information on the fitting process. If the LDCs were chosen incorrectly, we would obtain well-constrained model parameters with comparably small credibility intervals, which, however, could be inconsistent. We therefore

additionally fitted quadratic LDCs, assuming uniform priors on  $u_1$  and  $u_2$ , and performed an MCMC error analysis of the complete set of parameters. Our best-fit solution is determined by those parameter values that minimize the deviance after  $10^6$  iterations of the sampler. The errors are calculated from 68.3 % HPD intervals of the posterior probability distributions for the parameters. Our results are summarized in the upper part of Table 4.

Given their credibility intervals the parameters of our global fit are compatible with those by Southworth (2011) and Kipping & Bakos (2011b). We note a slight discrepancy with the results by Kipping & Bakos (2011b), who obtain a slightly larger radius ratio,  $p$ , of 0.1282. A small, possibly systematic discrepancy compared to the values of Kipping & Bakos (2011b) has also been noted by Southworth (2011). Within their  $2\sigma$  error intervals our LDCs are still consistent with the best-fit solution obtained by Kipping & Bakos (2011b), who found LDCs of  $u_1 = 0.52$  and  $u_2 = 0.06$ . We note that the sum,  $u_1 + u_2$ , of the LDCs is very well constrained in agreement with our considerations in Sec. 2.1.

As discussed in Howarth (2011b) we cannot directly compare our best-fit LDCs to predictions based on the stellar atmosphere model. This is due to the fact that we are fitting photometric data from a real star, using a simplified model of the stellar limb darkening. The high impact parameter of TrES-2b together with the fitting approach inevitably lead to considerable deviations of the photometrically determined LDCs from model-atmosphere characterizations. Instead, Howarth (2011b) proposes to compare the results from the photometric analysis with the results obtained from synthetic photometry based on a given atmosphere model (termed "SPAM"). Figure 1 shows the result of this consideration. The lowest deviance combination of LDCs after  $10^6$  MCMC samples is obviously inconsistent if compared directly to the predictions by Claret & Bloemen (2011) based on PHOENIX model atmospheres for TrES-2. However, the SPAM model based on the same model atmosphere is consistent with the best-fit LDCs. This strengthens our confidence in the reliability of the theoretically calculated LDCs.

Note that the simplified prescription of limb darkening used in our model also introduces small, but non-negligible systematic errors in the remaining light curve parameters due to the strong correlations between all parameters. In the following we therefore use the four-parametric, non-linear limb-darkening law proposed by Claret & Bloemen (2011), holding the LDCs fixed at their theoretically expected values to obtain the remaining transit parameters. This, of course, substantially reduces the errors on our parameter estimates because the strong correlations mediated by the limb-darkening treatment diminish. Our results after  $10^6$  iterations of the MCMC sampler are summarized in the lower part of Table 4.

##### 4.2. Secular change in inclination

The values inferred from the fit to the *Kepler* data are the most robust estimates of the planetary parameters of TrES-2 currently available. In the following, we reanalyze all publicly available photometric data of TrES-2 examining each transit separately to search for secular variations of the orbital inclination.

Secular inclination changes are empirically detectable as changes in transit duration, which is a function of  $a/R_s$ ,  $p$  and  $i$  (Seager & Mallén-Ornelas 2003). While each of these parameters may itself exhibit secular changes resulting in changes in the transit duration (Kipping 2010), we focus in the following on changes in the orbital inclination,  $i$ , and the time of transit minimum,  $\tau$ , of each transit. We thereby assume that neither the ra-

**Table 4.** Lowest-deviance parameters for the *Kepler* data after  $10^6$  MCMC samples compared to the results with fixed limb-darkening coefficients. Both fits assume a third light contribution according to Table 2.

Parameter	Value	Error (68.3 % HPD)
$i$ (°)	83.874	[ 83.806 , 83.910 ]
$p$	0.1257	[ 0.1240 , 0.1265 ]
$a/R_s$	7.903	[ 7.835 , 7.937 ]
$u_1$	0.19	[ -0.10 , 0.36 ]
$u_2$	0.43	[ 0.25 , 0.75 ]
$u_1 + u_2$	0.626	[0.605, 0.648]
$i$ (°)	83.9788	[ 83.9740 , 83.9837 ]
$p$	0.12759	[ 0.12755 , 0.12762 ]
$a/R_s$	7.9899	[ 7.9856 , 7.9943 ]
$a_1, a_2, a_3, a_4$	fixed, see Table 2	

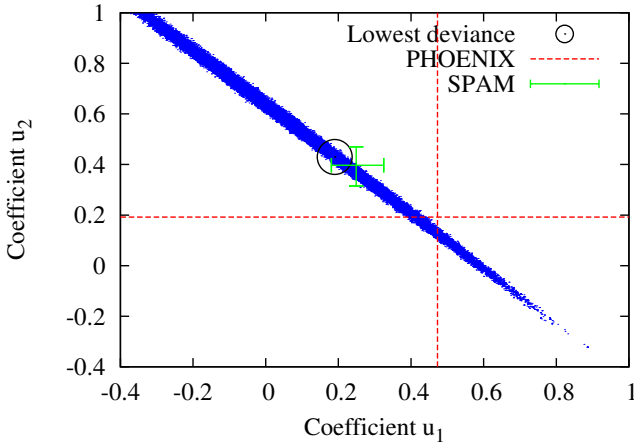


**Fig. 1.** Correlation between linear and quadratic limb-darkening coefficient resulting from  $10^6$  MCMC runs. The lowest deviance combination of parameters (circle) is significantly offset from the Claret & Bloemen (2011) model prediction (dashed red) but consistent with the result obtained from fitting synthetic photometry based on the same atmosphere model (SPAM, green).

**Table 5.** Prior information used for the MCMC calculations in Sec. 4.2.

Quantity	Prior	Source
$a/R_s$	$7.9899 \pm 0.0043$	Table 4
$p$	$0.127585 \pm 0.000035$	Table 4
$\tau$	uniform	
$i$	uniform	
$a_1, a_2, a_3, a_4$	fixed	Table 2
$L_3$	fixed	Table 2
$e$	0 (fixed)	

dius ratio nor the planetary orbit change in size over the course of the observations and that the orbit is circular. However, we still must account for our incomplete knowledge of the true value of  $a/R_s$  and  $p$ . We therefore leave both parameters free during the MCMC calculations imposing Gaussian priors according to the errors obtained from our global fit. Depending on the instrumental setup of the observations (cf. Table 3) we take into account the expected third light contribution and the LDCs according to Table 2. For each transit we obtain the posterior distributions for both  $\tau$  and  $i$  using  $10^4$  iterations of the MCMC sampler. We

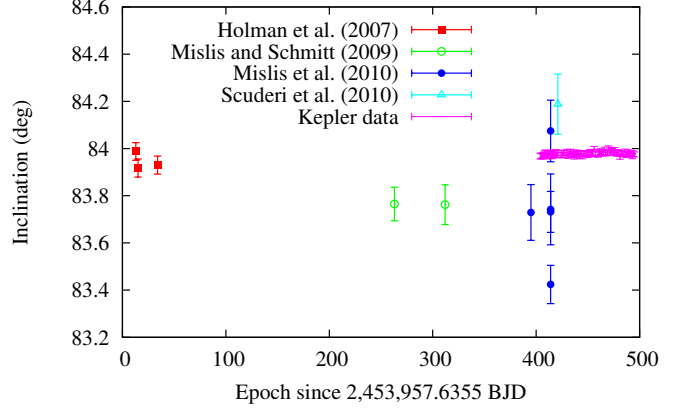


**Fig. 2.** Inclination versus transit epoch for TrES-2 based on publicly available ground-based data and the *Kepler* observations. Errors are derived from 95.5 % HPD intervals corresponding to  $2\sigma$  errors based on  $10^4$  MCMC iterations for each transit.

summarize the prior information in Table 5. The errors again correspond to 68.3 % HPD intervals.

Concerning the *Kepler* data, Kipping & Bakos (2011b) did not find evidence for parameter changes within the first two quarters. However, the public release of the last two quarters, i.e. quarters Q2 and Q3, provided a substantial enlargement of the data set. We therefore reanalyze the complete Q0 to Q3 set of transits in detail searching for variations of the inclination or transit timing variations (TTVs).

Our results are shown in Fig. 2. The superior quality of the *Kepler* data manifests itself in very small credibility intervals for these observations. While the data by Holman et al. (2007) are fully consistent with the inclination obtained by *Kepler*, we find systematically lower inclinations for the data sets of Mislis & Schmitt (2009) and Mislis et al. (2010). In fact, ignoring the *Kepler* data, the secular inclination change detected by Mislis & Schmitt (2009) is clearly visible.

Note, however, that our common fitting approach based on the results from *Kepler* and including the third light contribution yields best-fit values for the inclinations derived from the ground-based measurements that are closer to the *Kepler* values than those originally obtained by Mislis & Schmitt (2009) and Mislis et al. (2010). Furthermore, our new errors are quite large so that the *Kepler* value lies only just outside of our  $3\sigma$  error.

We also checked, whether it is possible to completely reconcile the *Kepler* observations with the results by Mislis & Schmitt (2009) and Mislis et al. (2010). Accounting for the possibility of normalization problems during data reduction we introduce an additional normalization constant to our model. Including this constant as another parameter of our MCMC marginally enlarges the uncertainties on the inclinations. We thus do not expect the deviation to stem from simple normalization problems.

Another cause for erroneous results would result from incorrectly taking into account the contribution of the contaminating third light. To fully reconcile the inclinations by Mislis & Schmitt (2009) and Mislis et al. (2010) with the best-fit inclination from the *Kepler* data would require contributions of a third light of 10 to 20 % of the total flux, which can be excluded from the observations by Daemgen et al. (2009). However, assuming a uniform prior for the third light contribution and demanding it to be smaller than 10 %, the credibility intervals become substantially larger including the *Kepler* result. We thus conclude, that

problems with the flux calibration possibly caused by the reference star are the most likely cause for the observed deviations.

In either case, the Kepler data rule out a decrease in inclination of the size expected by [Mislis et al. \(2010\)](#). The exact reason for their systematic deviation remains unclear. The [Holman et al. \(2007\)](#) data are consistent with the first four quarters of *Kepler* data. Note, however, that despite the long available time baseline the errors of the [Holman et al. \(2007\)](#) data points are too large to draw significant conclusions on the presence of other, smaller linear trends.

#### 4.3. Variability in the Kepler data

We now focus on the Kepler data searching for small trends or variations, which could still be consistent with the previous ground-based observations. Fig. 3 shows an enlarged view of the Kepler data; the errors are derived from the 68.3% HPD intervals, so they are equivalent to  $1\sigma$  errors.

We found a slight linear trend in the *Kepler* data. An MCMC analysis yields a slightly non-zero slope of  $(0.8 \pm 0.2) \times 10^{-4}$  /cycle. This would correspond to a secular inclination change nearly two orders of magnitude smaller than the value by [Mislis et al. \(2010\)](#). Extrapolating this trend back to the epoch of transit observations obtained by [Holman et al. \(2007\)](#), we would expect an inclination of  $83.94^\circ \pm 0.01^\circ$  consistent with the measurement errors.

In order to quantify the improvement of the different fits, we calculated the statistic

$$\hat{F} = \frac{(\chi_a^2 - \chi_b^2) / (v_a - v_b)}{\chi_b^2 / v_b} \quad (3)$$

and compared its value to an  $F$ -distribution with  $v_a - v_b$  and  $v_b$  degrees of freedom (e.g., [Rawlings et al. 1998](#)). We obtain a  $p$ -value of 0.004 indicating that the linear trend provides a better description compared to the constant at the  $2.8\sigma$  level, which we consider as indicative, but not significant evidence for the presence of such a trend.

After subtracting the linear trend from the data, we computed an error-weighted Lomb-Scargle periodogram ([Zechmeister & Kürster 2009](#)), which displays a single signal at a period of 45 cycles or 111 days with a false-alarm probability below 10%. Fig. 3 shows our best-fit sinusoidal model including a linear trend. An  $F$ -test comparing the model to the constant model yields a  $p$ -value of 0.015 (or  $2.4\sigma$ ); the test thus indicates the presence of an additional sinusoidal modulation superimposed on the linear trend, which however remains insignificant.

We can also compare the three models using the Bayesian information criterion,  $\text{BIC} = \chi^2 + k \ln N$  ([Schwarz 1978](#)), which penalizes the number  $k$  of model parameters given  $N = 81$  data points. We obtain BICs of 136.3, 127.6, and 117.0 for the constant, the linear trend, and the sinusoid with linear trend, respectively.

Despite being close to formal significance the signal is easily obliterated by the noise and could be introduced by some subtleties in our analysis. Assuming the sinusoidal model with linear trend to be true, we averaged two sets of 10 transits pertaining to low (around epoch 409, compare Fig. 3) and high (around epoch 470) inclinations, respectively. Subtracting both templates, their difference should exhibit a characteristic signature, which we model by subtracting two model calculations for  $i_L = 83.97^\circ$  and  $i_H = 83.99^\circ$ . We show the averaged templates together with their difference and the model in Fig. 4. While during ingress the flux difference shows a decrease following

the difference model, the signature during egress is obliterated by the noise. We checked that averaging transits pertaining to epochs close to the zero-crossing points of the sinusoidal model yields no substantial deviation from a constant.

We repeated our analysis using simulated control data to check, whether the signal is introduced by our data reduction or by “phasing effects” due to the *Kepler* cadence ([Kipping & Bakos 2011a](#)). However, we could not detect similar signals exceeding the noise. We further changed our data normalization strategy (see Sec. 3), but found the variation of inclination to be stable against these changes. Analyzing similar *Kepler* targets we found spurious periodicities in some cases, which, however, remained insignificant in the periodogram (at false-alarm probabilities above 10%). In summary, there seem to be some indications for a short-term inclination variation and an underlying secular change in the *Kepler* data of TrES-2. However, the detected signal is merely an indication of inclination changes in the *Kepler* data, because in the baseline of space-based observations is still too short to draw significant conclusions on the stability or variability in the inclination (compare Fig. 4).

Turning to the times of transit minimum of the Kepler transits, Fig. 5 shows that the transit timing is consistent with being constant over the course of the *Kepler* data. An  $F$ -test comparing the constant and a linear model yields a  $p$ -value of 0.92; thus, there is no evidence for a linear trend. In the periodogram there is no signal at false-alarm probabilities below 10%. We thus do not see any evidence for TTVs in the *Kepler* data.

The apparent secular change in inclination refers to the orientation of the orbital plane of TrES-2b relative to the observer’s tangential plane and, assuming a circular orbit, can be interpreted as nodal regression at fixed orbit inclination. While gravitational perturbation due to an oblate host star is unlikely given that TrES-2A is a slow rotator very similar to the Sun ([Mislis et al. 2010](#)), additional bodies in the stellar system could offer a viable explanation for secular changes in the orbital parameters. If we assume our linear trend in inclination to be physical, we can estimate the period of a perturber of specified mass in a circular, coplanar orbit using Eq. 13 in [Mislis et al. \(2010\)](#). We find that a perturbing planet of Jovian mass would be expected at orbital periods between 100 and 300 days. However, a perturbing second planet capable of causing nodal precession of the transiting planet would also be expected to induce short-term periodic variations of its orbital elements ([Holman & Murray 2005](#); [Agol et al. 2005](#)). To calculate the amplitude of such TTVs, we use an approach based on analytic perturbation theory developed by [Nesvorný & Morbidelli \(2008\)](#). Outside possible mean-motion resonances additional Jovian mass bodies with periods larger than 100 days would cause a TTV amplitude below 1 s if on a circular orbit. Given the standard deviation of the times of transit minimum of 4.8 s, such a TTV amplitude cannot be ruled out. Thus, the existence of an external perturber in the system still provides an entirely plausible scenario.

## 5. Summary and Conclusion

We presented an analysis of all publicly available photometric data obtained during planetary transits of TrES-2b including four quarters of data obtained with the *Kepler* space telescope. The transits were fitted in a common scheme using theoretically calculated LDCs and taking into account the contribution of a third light.

Fitting quarters Q0 to Q3 of the *Kepler* data, we were able to refine the system parameters determined by [Kipping & Bakos \(2011b\)](#) and [Southworth \(2011\)](#). Our results are compatible with

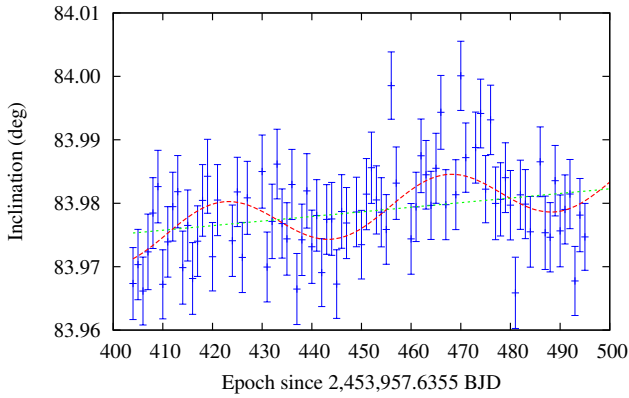


**Fig. 3.** Inclination versus transit epoch for the *Kepler* observations. Errors are computed from the 68.3 % HPD intervals based on  $10^4$  MCMC iterations for each transit. The best-fitting linear (dotted/green) and sinusoidal models including a linear trend (dashed/red) are overlotted.

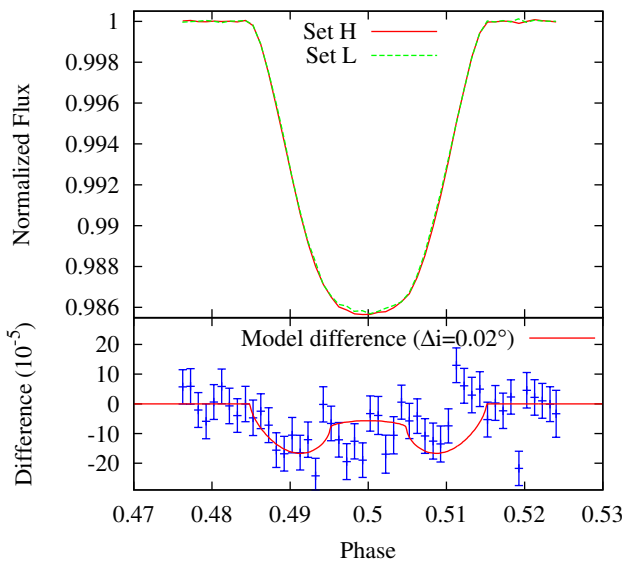


**Fig. 4.** *Upper panel:* Averaged templates of two sets of 10 transits with high (H, solid red) and low (L, dashed green) inclinations, respectively, as expected from the tentative sinusoidal variation of the inclinations obtained by *Kepler*. *Lower panel:* The difference between the two averaged transits. The expected difference for two models pertaining to  $i = 83.97^\circ$  and  $83.99^\circ$  is shown for reference (solid red).

these previous studies, our errors being slightly smaller. Its high impact parameter makes the TrES-2-system sensitive to details of the adopted stellar limb-darkening model because only the covered regions close to the stellar limb are used to extrapolate the limb darkening for the whole stellar disk. Small differences between limb-darkening prescriptions therefore yield significant differences in the resulting best fits. We find that the theoretically calculated LDCs by Claret & Bloemen (2011) provide a correct description of the observed limb darkening if compared with the data via the SPAM approach as advocated by Howarth (2011b).

The data by Mislis & Schmitt (2009) and Mislis et al. (2010) are found to be inconsistent with the remaining data, especially the *Kepler* data. The discrepancy can neither be attributed to er-

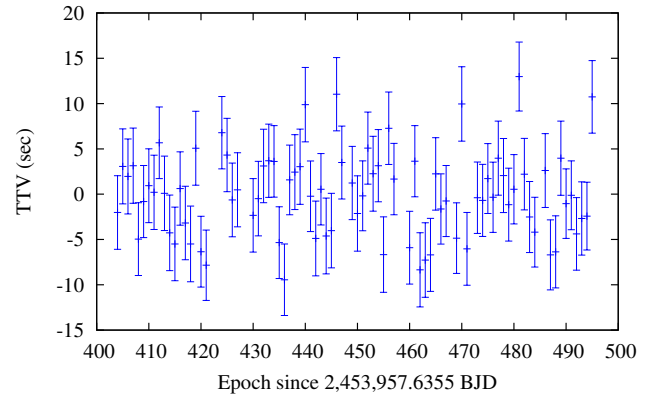


**Fig. 5.** Transit timing variation (TTV) versus transit epoch for TrES-2b using the best-fit ephemerides. Errors are computed from the 68.3 % HPD intervals based on  $10^4$  MCMC iterations for each transit.

rors in the theoretical LDCs nor to the contribution of third light, which the original studies did not account for. The most probable explanations would be subtleties in the data reduction, perhaps due to problems with the reference star, or the presence of time-correlated noise yielding underestimated parameter errors (Carter & Winn 2009).

Excluding the Mislis & Schmitt (2009) and Mislis et al. (2010) data sets, all observations can be reconciled in a consistent picture. The extension of the available *Kepler* data by two additional quarters reveal some hints for systematic variations in the inclination, the marginally significant slope would be consistent with the data by Holman et al. (2007). However, given the available baseline of space-based observations we consider the inclination change as indicative but not significant. Further data, which already have been obtained by the *Kepler* space telescope, will settle this issue in the near future.

Our study shows that space-based and ground-based photometry of TrES-2 can be analyzed in a common scheme yielding consistent results. While space-based photometry offers the possibility to constrain all system parameters at once, with the eventual decommissioning of *Kepler* it will again be up to ground-based measurements to search for long-term changes in the orbital parameters of TrES-2.

*Acknowledgements.* This paper includes data collected by the Kepler mission. Funding for the Kepler mission is provided by the NASA Science Mission Directorate. The Kepler observations were obtained from the Multimission Archive at the Space Telescope Science Institute (MAST). H.M.M. is supported in the framework of the DFG-funded Research Training Group “Extrasolar Planets and their Host Stars” (DFG 1351/2). S.S. acknowledges support from the DLR under grant 50OR0703.

## References

- Agol, E., Steffen, J., Sari, R., & Clarkson, W. 2005, *MNRAS*, 359, 567  
 Ammler-von Eiff, M., Santos, N. C., Sousa, S. G., et al. 2009, *A&A*, 507, 523  
 Carter, J. A. & Winn, J. N. 2009, *ApJ*, 704, 51  
 Christiansen, J. L., Ballard, S., Charbonneau, D., et al. 2011, *ApJ*, 726, 94  
 Claret, A. & Bloemen, S. 2011, *A&A*, 529, A75  
 Daemgen, S., Hormuth, F., Brandner, W., et al. 2009, *A&A*, 498, 567  
 Eastman, J., Siverd, R., & Gaudi, B. S. 2010, *PASP*, 122, 935  
 Gilliland, R. L., Jenkins, J. M., Borucki, W. J., et al. 2010, *ApJ*, 713, L160  
 Haario, H., Saksman, E., & Tamminen, J. 2001, *Bernoulli*, 7 (2), 223  
 Holman, M. J. & Murray, N. W. 2005, *Science*, 307, 1288  
 Holman, M. J., Winn, J. N., Latham, D. W., et al. 2007, *ApJ*, 664, 1185  
 Howarth, I. D. 2011a, *MNRAS*, 413, 1515  
 Howarth, I. D. 2011b, *MNRAS*, 1572

- Jones, E., Oliphant, T., Peterson, P., et al. 2001, SciPy: Open source scientific tools for Python, <http://www.scipy.org>
- Kipping, D. & Bakos, G. 2011a, ApJ, 730, 50
- Kipping, D. & Bakos, G. 2011b, ApJ, 733, 36
- Kipping, D. M. 2010, MNRAS, 407, 301
- Makhoul, J. 1980, Acoustics, Speech and Signal Processing, IEEE Transactions on, 28, 27
- Mandel, K. & Agol, E. 2002, ApJ, 580, L171
- Mislis, D. & Schmitt, J. H. M. M. 2009, A&A, 500, L45
- Mislis, D., Schröter, S., Schmitt, J. H. M. M., Cordes, O., & Reif, K. 2010, A&A, 510, A107
- Nesvorný, D. & Morbidelli, A. 2008, ApJ, 688, 636
- O'Donovan, F. T., Charbonneau, D., Mandushev, G., et al. 2006, ApJ, 651, L61
- Pál, A. 2008, MNRAS, 390, 281
- Patil, A., Huard, D., & Fannesbeck, C. J. 2010, Journal of Statistical Software, 35, 1
- Rabus, M., Deeg, H. J., Alonso, R., Belmonte, J. A., & Almenara, J. M. 2009, A&A, 508, 1011
- Raetz, S., Maciejewski, G., Mugrauer, M., et al. 2011, Detection and Dynamics of Transiting Exoplanets, St. Michel l'Observatoire, France, Edited by F. Bouchy; R. Díaz; C. Moutou; EPJ Web of Conferences, Volume 11, id.05007, 11, 5007
- Raetz, S., Mugrauer, M., Schmidt, T. O. B., et al. 2009, Astronomische Nachrichten, 330, 459
- Rawlings, J. O., Pantula, S. G., & Dickey, D. A. 1998, Applied regression analysis, 2nd edn., Springer texts in statistics (New York, NY: Springer)
- Schwarz, G. 1978, The Annals of Statistics, 6, 461
- Scuderi, L. J., Dittmann, J. A., Males, J. R., Green, E. M., & Close, L. M. 2010, ApJ, 714, 462
- Seager, S. & Mallén-Ornelas, G. 2003, ApJ, 585, 1038
- Southworth, J. 2008, MNRAS, 386, 1644
- Southworth, J. 2010, MNRAS, 408, 1689
- Southworth, J. 2011, MNRAS, 417, 2166
- Sozzetti, A., Torres, G., Charbonneau, D., et al. 2007, ApJ, 664, 1190
- Vihola, M. 2011, Stochastic Processes and their Applications, 121, 2839
- Welsh, W. F., Orosz, J. A., Seager, S., et al. 2010, ApJ, 713, L145
- Zechmeister, M. & Kürster, M. 2009, A&A, 496, 577



## **Appendix A: Results from individual fits**

In Table A.1, we show the transit parameters of TrES-2b from individual fits of ground-based and *Kepler* data.

**Table A.1.** Transit parameters for TrES-2b from individual fits of ground-based and *Kepler* data. Epoch refers to the first transit of TrES-2b observed by O'Donovan et al. (2006). For the MCMC analysis, we fix the limb-darkening coefficients corresponding to the filter band (cf. Table 2) and use prior information as described in Table 5.

Epoch	$\tau$ [BJD <sub>TDB</sub> - 2, 450, 000 d]	$i$ [deg]	$a/R_s$	$p$	Reference
Publicly available ground-based data					
13	3989.752878 <sup>+0.000208</sup> <sub>-0.000233</sub>	83.9876 <sup>+0.0171</sup> <sub>-0.0201</sub>	7.9899 <sup>+0.0038</sup> <sub>-0.0047</sub>	0.127585 <sup>+0.000034</sup> <sub>-0.000035</sub>	Holman et al. (2007)
15	3994.694003 <sup>+0.000233</sup> <sub>-0.000227</sub>	83.9174 <sup>+0.0166</sup> <sub>-0.0219</sub>	7.9898 <sup>+0.0042</sup> <sub>-0.0044</sub>	0.127585 <sup>+0.000038</sup> <sub>-0.000033</sub>	Holman et al. (2007)
34	4041.635919 <sup>+0.000213</sup> <sub>-0.000255</sub>	83.9300 <sup>+0.0184</sup> <sub>-0.0198</sub>	7.9893 <sup>+0.0042</sup> <sub>-0.0041</sub>	0.127582 <sup>+0.000039</sup> <sub>-0.000031</sub>	Holman et al. (2007)
263	4607.398143 <sup>+0.000512</sup> <sub>-0.000574</sub>	83.7650 <sup>+0.0378</sup> <sub>-0.0332</sub>	7.9897 <sup>+0.0042</sup> <sub>-0.0043</sub>	0.127585 <sup>+0.000037</sup> <sub>-0.000034</sub>	Mislis & Schmitt (2009)
312	4728.465365 <sup>+0.000596</sup> <sub>-0.000580</sub>	83.7622 <sup>+0.0430</sup> <sub>-0.0413</sub>	7.9895 <sup>+0.0040</sup> <sub>-0.0042</sub>	0.127581 <sup>+0.000036</sup> <sub>-0.000034</sub>	Mislis & Schmitt (2009)
395	4933.527211 <sup>+0.000743</sup> <sub>-0.000861</sub>	83.7291 <sup>+0.0602</sup> <sub>-0.0579</sub>	7.9897 <sup>+0.0039</sup> <sub>-0.0045</sub>	0.127584 <sup>+0.000037</sup> <sub>-0.000034</sub>	Mislis et al. (2010)
414	4980.466843 <sup>+0.000712</sup> <sub>-0.000717</sub>	83.4239 <sup>+0.0455</sup> <sub>-0.0358</sub>	7.9897 <sup>+0.0040</sup> <sub>-0.0046</sub>	0.127583 <sup>+0.000034</sup> <sub>-0.000036</sub>	Mislis et al. (2010)
414	4980.467292 <sup>+0.000552</sup> <sub>-0.000648</sub>	83.7314 <sup>+0.0427</sup> <sub>-0.0440</sub>	7.9896 <sup>+0.0038</sup> <sub>-0.0048</sub>	0.127582 <sup>+0.000034</sup> <sub>-0.000037</sub>	Mislis et al. (2010)
414	4980.467765 <sup>+0.001166</sup> <sub>-0.001178</sub>	84.0745 <sup>+0.0579</sup> <sub>-0.0726</sub>	7.9897 <sup>+0.0039</sup> <sub>-0.0045</sub>	0.127585 <sup>+0.000036</sup> <sub>-0.000034</sub>	Mislis et al. (2010)
414	4980.467504 <sup>+0.001041</sup> <sub>-0.001389</sub>	83.7421 <sup>+0.0780</sup> <sub>-0.0723</sub>	7.9900 <sup>+0.0044</sup> <sub>-0.0044</sub>	0.127585 <sup>+0.000035</sup> <sub>-0.000037</sub>	Mislis et al. (2010)
421	4997.762881 <sup>+0.000642</sup> <sub>-0.000820</sub>	84.1880 <sup>+0.0659</sup> <sub>-0.0616</sub>	7.9900 <sup>+0.0046</sup> <sub>-0.0040</sub>	0.127587 <sup>+0.000037</sup> <sub>-0.000033</sub>	Scuderi et al. (2010)
<i>Kepler</i> data					
404	4955.763245 <sup>+0.000050</sup> <sub>-0.000044</sub>	83.9673 <sup>+0.0047</sup> <sub>-0.0066</sub>	7.9883 <sup>+0.0044</sup> <sub>-0.0044</sub>	0.127577 <sup>+0.000037</sup> <sub>-0.000034</sub>	
405	4958.233917 <sup>+0.000047</sup> <sub>-0.000048</sub>	83.9703 <sup>+0.0055</sup> <sub>-0.0056</sub>	7.9886 <sup>+0.0044</sup> <sub>-0.0041</sub>	0.127579 <sup>+0.000036</sup> <sub>-0.000032</sub>	
406	4960.704517 <sup>+0.000042</sup> <sub>-0.000054</sub>	83.9662 <sup>+0.0052</sup> <sub>-0.0055</sub>	7.9886 <sup>+0.0039</sup> <sub>-0.0041</sub>	0.127575 <sup>+0.000034</sup> <sub>-0.000034</sub>	
407	4963.175144 <sup>+0.000040</sup> <sub>-0.000056</sub>	83.9723 <sup>+0.0063</sup> <sub>-0.0056</sub>	7.9897 <sup>+0.0042</sup> <sub>-0.0047</sub>	0.127577 <sup>+0.000031</sup> <sub>-0.000036</sub>	
408	4965.645664 <sup>+0.000048</sup> <sub>-0.000045</sub>	83.9784 <sup>+0.0056</sup> <sub>-0.0056</sub>	7.9901 <sup>+0.0046</sup> <sub>-0.0040</sub>	0.127578 <sup>+0.000037</sup> <sub>-0.000036</sub>	
409	4968.116325 <sup>+0.000048</sup> <sub>-0.000044</sub>	83.9826 <sup>+0.0062</sup> <sub>-0.0052</sub>	7.9900 <sup>+0.0046</sup> <sub>-0.0039</sub>	0.127580 <sup>+0.000037</sup> <sub>-0.000033</sub>	
410	4970.586959 <sup>+0.000043</sup> <sub>-0.000051</sub>	83.9672 <sup>+0.0056</sup> <sub>-0.0053</sub>	7.9899 <sup>+0.0040</sup> <sub>-0.0043</sub>	0.127587 <sup>+0.000038</sup> <sub>-0.000031</sub>	
411	4973.057564 <sup>+0.000052</sup> <sub>-0.000043</sub>	83.9739 <sup>+0.0049</sup> <sub>-0.0062</sub>	7.9876 <sup>+0.0047</sup> <sub>-0.0036</sub>	0.127570 <sup>+0.000039</sup> <sub>-0.000032</sub>	
412	4975.528240 <sup>+0.000043</sup> <sub>-0.000048</sub>	83.9795 <sup>+0.0052</sup> <sub>-0.0056</sub>	7.9891 <sup>+0.0037</sup> <sub>-0.0043</sub>	0.127578 <sup>+0.000036</sup> <sub>-0.000034</sub>	
413	4977.998789 <sup>+0.000047</sup> <sub>-0.000048</sub>	83.9818 <sup>+0.0058</sup> <sub>-0.0056</sub>	7.9904 <sup>+0.0049</sup> <sub>-0.0036</sub>	0.127589 <sup>+0.000037</sup> <sub>-0.000034</sub>	
414	4980.469352 <sup>+0.000045</sup> <sub>-0.000051</sub>	83.9698 <sup>+0.0060</sup> <sub>-0.0055</sub>	7.9893 <sup>+0.0041</sup> <sub>-0.0044</sub>	0.127570 <sup>+0.000032</sup> <sub>-0.000035</sub>	
415	4982.939951 <sup>+0.000047</sup> <sub>-0.000047</sub>	83.9765 <sup>+0.0061</sup> <sub>-0.0051</sub>	7.9874 <sup>+0.0037</sup> <sub>-0.0045</sub>	0.127569 <sup>+0.000038</sup> <sub>-0.000031</sub>	
416	4985.410635 <sup>+0.000047</sup> <sub>-0.000047</sub>	83.9681 <sup>+0.0056</sup> <sub>-0.0057</sub>	7.9900 <sup>+0.0037</sup> <sub>-0.0048</sub>	0.127581 <sup>+0.000037</sup> <sub>-0.000033</sub>	
417	4987.881204 <sup>+0.000046</sup> <sub>-0.000048</sub>	83.9740 <sup>+0.0055</sup> <sub>-0.0056</sub>	7.9904 <sup>+0.0038</sup> <sub>-0.0044</sub>	0.127585 <sup>+0.000036</sup> <sub>-0.000033</sub>	
418	4990.351791 <sup>+0.000048</sup> <sub>-0.000048</sub>	83.9804 <sup>+0.0053</sup> <sub>-0.0060</sub>	7.9896 <sup>+0.0042</sup> <sub>-0.0043</sub>	0.127580 <sup>+0.000037</sup> <sub>-0.000031</sub>	
419	4992.822527 <sup>+0.000042</sup> <sub>-0.000052</sub>	83.9843 <sup>+0.0054</sup> <sub>-0.0062</sub>	7.9896 <sup>+0.0048</sup> <sub>-0.0038</sub>	0.127576 <sup>+0.000036</sup> <sub>-0.000035</sub>	
420	4995.293008 <sup>+0.000044</sup> <sub>-0.000046</sub>	83.9716 <sup>+0.0051</sup> <sub>-0.0057</sub>	7.9890 <sup>+0.0041</sup> <sub>-0.0040</sub>	0.127578 <sup>+0.000035</sup> <sub>-0.000032</sub>	
421	4997.763604 <sup>+0.000045</sup> <sub>-0.000045</sub>	83.9805 <sup>+0.0051</sup> <sub>-0.0062</sub>	7.9895 <sup>+0.0039</sup> <sub>-0.0043</sub>	0.127578 <sup>+0.000038</sup> <sub>-0.000032</sub>	
424	5005.175613 <sup>+0.000049</sup> <sub>-0.000044</sub>	83.9741 <sup>+0.0063</sup> <sub>-0.0049</sub>	7.9900 <sup>+0.0041</sup> <sub>-0.0041</sub>	0.127589 <sup>+0.000033</sup> <sub>-0.000036</sub>	
425	5007.646198 <sup>+0.000045</sup> <sub>-0.000049</sub>	83.9818 <sup>+0.0053</sup> <sub>-0.0056</sub>	7.9884 <sup>+0.0043</sup> <sub>-0.0041</sub>	0.127577 <sup>+0.000037</sup> <sub>-0.000032</sub>	
426	5010.116754 <sup>+0.000047</sup> <sub>-0.000047</sub>	83.9715 <sup>+0.0055</sup> <sub>-0.0056</sub>	7.9904 <sup>+0.0043</sup> <sub>-0.0039</sub>	0.127583 <sup>+0.000040</sup> <sub>-0.000029</sub>	
427	5012.587380 <sup>+0.000045</sup> <sub>-0.000050</sub>	83.9809 <sup>+0.0056</sup> <sub>-0.0059</sub>	7.9899 <sup>+0.0045</sup> <sub>-0.0041</sub>	0.127583 <sup>+0.000030</sup> <sub>-0.000038</sub>	
430	5019.999187 <sup>+0.000042</sup> <sub>-0.000052</sub>	83.9850 <sup>+0.0055</sup> <sub>-0.0060</sub>	7.9895 <sup>+0.0048</sup> <sub>-0.0045</sub>	0.127589 <sup>+0.000032</sup> <sub>-0.000036</sub>	
431	5022.469822 <sup>+0.000051</sup> <sub>-0.000044</sub>	83.9700 <sup>+0.0052</sup> <sub>-0.0058</sub>	7.9901 <sup>+0.0039</sup> <sub>-0.0044</sub>	0.127589 <sup>+0.000037</sup> <sub>-0.000033</sub>	
432	5024.940477 <sup>+0.000050</sup> <sub>-0.000044</sub>	83.9771 <sup>+0.0051</sup> <sub>-0.0067</sub>	7.9892 <sup>+0.0043</sup> <sub>-0.0046</sub>	0.127581 <sup>+0.000040</sup> <sub>-0.000030</sub>	
433	5027.411097 <sup>+0.000046</sup> <sub>-0.000047</sub>	83.9862 <sup>+0.0050</sup> <sub>-0.0060</sub>	7.9897 <sup>+0.0041</sup> <sub>-0.0041</sub>	0.127579 <sup>+0.000035</sup> <sub>-0.000036</sub>	
434	5029.881709 <sup>+0.000043</sup> <sub>-0.000048</sub>	83.9768 <sup>+0.0054</sup> <sub>-0.0055</sub>	7.9887 <sup>+0.0040</sup> <sub>-0.0043</sub>	0.127577 <sup>+0.000034</sup> <sub>-0.000037</sub>	
435	5032.352219 <sup>+0.000047</sup> <sub>-0.000045</sub>	83.9744 <sup>+0.0057</sup> <sub>-0.0058</sub>	7.9899 <sup>+0.0041</sup> <sub>-0.0044</sub>	0.127580 <sup>+0.000038</sup> <sub>-0.000032</sub>	
436	5034.822785 <sup>+0.000047</sup> <sub>-0.000045</sub>	83.9830 <sup>+0.0052</sup> <sub>-0.0058</sub>	7.9906 <sup>+0.0039</sup> <sub>-0.0045</sub>	0.127587 <sup>+0.000032</sup> <sub>-0.000035</sub>	
437	5037.293526 <sup>+0.000042</sup> <sub>-0.000047</sub>	83.9665 <sup>+0.0052</sup> <sub>-0.0060</sub>	7.9893 <sup>+0.0041</sup> <sub>-0.0042</sub>	0.127577 <sup>+0.000034</sup> <sub>-0.000036</sub>	
438	5039.764149 <sup>+0.000046</sup> <sub>-0.000049</sub>	83.9742 <sup>+0.0057</sup> <sub>-0.0056</sub>	7.9890 <sup>+0.0044</sup> <sub>-0.0041</sub>	0.127582 <sup>+0.000031</sup> <sub>-0.000038</sub>	
439	5042.234769 <sup>+0.000049</sup> <sub>-0.000047</sub>	83.9819 <sup>+0.0054</sup> <sub>-0.0063</sub>	7.9916 <sup>+0.0042</sup> <sub>-0.0046</sub>	0.127606 <sup>+0.000035</sup> <sub>-0.000036</sub>	
440	5044.705462 <sup>+0.000049</sup> <sub>-0.000046</sub>	83.9731 <sup>+0.0061</sup> <sub>-0.0054</sub>	7.9897 <sup>+0.0041</sup> <sub>-0.0044</sub>	0.127580 <sup>+0.000037</sup> <sub>-0.000034</sub>	
441	5047.175958 <sup>+0.000043</sup> <sub>-0.000047</sub>	83.9781 <sup>+0.0059</sup> <sub>-0.0054</sub>	7.9889 <sup>+0.0038</sup> <sub>-0.0047</sub>	0.127583 <sup>+0.000034</sup> <sub>-0.000035</sub>	

**Table A.1.** continued.

Epoch	$\tau$ [BJD <sub>TDB</sub> - 2,450,000 d]	$i$ [deg]	$a/R_s$	$p$	Reference
442	5049.646518 <sup>+0.000046</sup> <sub>-0.000050</sub>	83.9691 <sup>+0.0057</sup> <sub>-0.0050</sub>	7.9903 <sup>+0.0039</sup> <sub>-0.0042</sub>	0.127591 <sup>+0.000038</sup> <sub>-0.000032</sub>	
443	5052.117194 <sup>+0.000045</sup> <sub>-0.000046</sub>	83.9774 <sup>+0.0063</sup> <sub>-0.0047</sub>	7.9902 <sup>+0.0035</sup> <sub>-0.0047</sub>	0.127588 <sup>+0.000031</sup> <sub>-0.000038</sub>	
444	5054.587747 <sup>+0.000051</sup> <sub>-0.000046</sub>	83.9775 <sup>+0.0058</sup> <sub>-0.0057</sub>	7.9885 <sup>+0.0044</sup> <sub>-0.0042</sub>	0.127581 <sup>+0.000040</sup> <sub>-0.000030</sub>	
445	5057.058368 <sup>+0.000046</sup> <sub>-0.000049</sub>	83.9673 <sup>+0.0055</sup> <sub>-0.0054</sub>	7.9890 <sup>+0.0044</sup> <sub>-0.0039</sub>	0.127581 <sup>+0.000037</sup> <sub>-0.000034</sub>	
446	5059.529155 <sup>+0.000044</sup> <sub>-0.000049</sub>	83.9787 <sup>+0.0056</sup> <sub>-0.0060</sub>	7.9890 <sup>+0.0042</sup> <sub>-0.0045</sub>	0.127580 <sup>+0.000036</sup> <sub>-0.000033</sub>	
447	5061.999681 <sup>+0.000048</sup> <sub>-0.000045</sub>	83.9769 <sup>+0.0054</sup> <sub>-0.0057</sub>	7.9895 <sup>+0.0043</sup> <sub>-0.0042</sub>	0.127576 <sup>+0.000036</sup> <sub>-0.000035</sub>	
449	5066.940882 <sup>+0.000048</sup> <sub>-0.000045</sub>	83.9786 <sup>+0.0050</sup> <sub>-0.0060</sub>	7.9902 <sup>+0.0043</sup> <sub>-0.0041</sub>	0.127589 <sup>+0.000034</sup> <sub>-0.000036</sub>	
450	5069.411456 <sup>+0.000046</sup> <sub>-0.000050</sub>	83.9735 <sup>+0.0050</sup> <sub>-0.0058</sub>	7.9896 <sup>+0.0042</sup> <sub>-0.0041</sub>	0.127583 <sup>+0.000033</sup> <sub>-0.000036</sub>	
451	5071.882092 <sup>+0.000045</sup> <sub>-0.000044</sub>	83.9814 <sup>+0.0051</sup> <sub>-0.0061</sub>	7.9900 <sup>+0.0048</sup> <sub>-0.0038</sub>	0.127587 <sup>+0.000033</sup> <sub>-0.000035</sub>	
452	5074.352766 <sup>+0.000044</sup> <sub>-0.000048</sub>	83.9856 <sup>+0.0058</sup> <sub>-0.0054</sub>	7.9910 <sup>+0.0040</sup> <sub>-0.0046</sub>	0.127591 <sup>+0.000034</sup> <sub>-0.000033</sub>	
453	5076.823347 <sup>+0.000047</sup> <sub>-0.000048</sub>	83.9805 <sup>+0.0058</sup> <sub>-0.0050</sub>	7.9896 <sup>+0.0045</sup> <sub>-0.0035</sub>	0.127578 <sup>+0.000037</sup> <sub>-0.000032</sub>	
454	5079.293970 <sup>+0.000049</sup> <sub>-0.000043</sub>	83.9786 <sup>+0.0051</sup> <sub>-0.0058</sub>	7.9904 <sup>+0.0042</sup> <sub>-0.0042</sub>	0.127581 <sup>+0.000039</sup> <sub>-0.000029</sub>	
455	5081.764470 <sup>+0.000043</sup> <sub>-0.000054</sub>	83.9759 <sup>+0.0051</sup> <sub>-0.0059</sub>	7.9892 <sup>+0.0044</sup> <sub>-0.0038</sub>	0.127581 <sup>+0.000035</sup> <sub>-0.000035</sub>	
456	5084.235245 <sup>+0.000045</sup> <sub>-0.000048</sub>	83.9985 <sup>+0.0058</sup> <sub>-0.0048</sub>	7.9907 <sup>+0.0037</sup> <sub>-0.0043</sub>	0.127594 <sup>+0.000036</sup> <sub>-0.000032</sub>	
457	5086.705793 <sup>+0.000048</sup> <sub>-0.000044</sub>	83.9832 <sup>+0.0053</sup> <sub>-0.0061</sub>	7.9902 <sup>+0.0045</sup> <sub>-0.0040</sub>	0.127581 <sup>+0.000035</sup> <sub>-0.000034</sub>	
460	5094.117546 <sup>+0.000046</sup> <sub>-0.000047</sub>	83.9744 <sup>+0.0065</sup> <sub>-0.0046</sub>	7.9914 <sup>+0.0041</sup> <sub>-0.0043</sub>	0.127594 <sup>+0.000037</sup> <sub>-0.000033</sub>	
461	5096.588269 <sup>+0.000042</sup> <sub>-0.000049</sub>	83.9794 <sup>+0.0057</sup> <sub>-0.0052</sub>	7.9904 <sup>+0.0042</sup> <sub>-0.0039</sub>	0.127585 <sup>+0.000032</sup> <sub>-0.000038</sub>	
462	5099.058744 <sup>+0.000049</sup> <sub>-0.000046</sub>	83.9875 <sup>+0.0059</sup> <sub>-0.0057</sub>	7.9908 <sup>+0.0042</sup> <sub>-0.0048</sub>	0.127593 <sup>+0.000037</sup> <sub>-0.000034</sub>	
463	5101.529370 <sup>+0.000051</sup> <sub>-0.000044</sub>	83.9845 <sup>+0.0058</sup> <sub>-0.0051</sub>	7.9903 <sup>+0.0043</sup> <sub>-0.0043</sub>	0.127599 <sup>+0.000037</sup> <sub>-0.000032</sub>	
464	5103.999990 <sup>+0.000048</sup> <sub>-0.000045</sub>	83.9797 <sup>+0.0050</sup> <sub>-0.0058</sub>	7.9895 <sup>+0.0043</sup> <sub>-0.0041</sub>	0.127592 <sup>+0.000037</sup> <sub>-0.000033</sub>	
465	5106.470706 <sup>+0.000049</sup> <sub>-0.000043</sub>	83.9855 <sup>+0.0049</sup> <sub>-0.0061</sub>	7.9899 <sup>+0.0044</sup> <sub>-0.0041</sub>	0.127586 <sup>+0.000035</sup> <sub>-0.000035</sub>	
466	5108.941275 <sup>+0.000046</sup> <sub>-0.000044</sub>	83.9943 <sup>+0.0056</sup> <sub>-0.0061</sub>	7.9897 <sup>+0.0048</sup> <sub>-0.0037</sub>	0.127581 <sup>+0.000038</sup> <sub>-0.000030</sub>	
467	5111.411898 <sup>+0.000042</sup> <sub>-0.000048</sub>	83.9798 <sup>+0.0051</sup> <sub>-0.0059</sub>	7.9896 <sup>+0.0041</sup> <sub>-0.0044</sub>	0.127585 <sup>+0.000035</sup> <sub>-0.000037</sub>	
469	5116.353078 <sup>+0.000042</sup> <sub>-0.000048</sub>	83.9814 <sup>+0.0062</sup> <sub>-0.0049</sub>	7.9907 <sup>+0.0046</sup> <sub>-0.0039</sub>	0.127591 <sup>+0.000035</sup> <sub>-0.000033</sub>	
470	5118.823862 <sup>+0.000046</sup> <sub>-0.000049</sub>	84.0001 <sup>+0.0058</sup> <sub>-0.0051</sub>	7.9922 <sup>+0.0047</sup> <sub>-0.0038</sub>	0.127599 <sup>+0.000033</sup> <sub>-0.000038</sub>	
471	5121.294291 <sup>+0.000047</sup> <sub>-0.000046</sub>	83.9872 <sup>+0.0053</sup> <sub>-0.0056</sub>	7.9899 <sup>+0.0040</sup> <sub>-0.0046</sub>	0.127590 <sup>+0.000032</sup> <sub>-0.000036</sub>	
473	5126.235583 <sup>+0.000044</sup> <sub>-0.000047</sub>	83.9888 <sup>+0.0052</sup> <sub>-0.0061</sub>	7.9893 <sup>+0.0043</sup> <sub>-0.0040</sub>	0.127586 <sup>+0.000035</sup> <sub>-0.000037</sub>	
474	5128.706192 <sup>+0.000046</sup> <sub>-0.000046</sub>	83.9941 <sup>+0.0051</sup> <sub>-0.0058</sub>	7.9910 <sup>+0.0044</sup> <sub>-0.0036</sub>	0.127586 <sup>+0.000037</sup> <sub>-0.000033</sub>	
475	5131.176834 <sup>+0.000042</sup> <sub>-0.000047</sub>	83.9822 <sup>+0.0061</sup> <sub>-0.0045</sub>	7.9911 <sup>+0.0040</sup> <sub>-0.0039</sub>	0.127592 <sup>+0.000034</sup> <sub>-0.000035</sub>	
476	5133.647423 <sup>+0.000042</sup> <sub>-0.000048</sub>	83.9931 <sup>+0.0052</sup> <sub>-0.0058</sub>	7.9909 <sup>+0.0041</sup> <sub>-0.0041</sub>	0.127593 <sup>+0.000033</sup> <sub>-0.000035</sub>	
477	5136.118086 <sup>+0.000043</sup> <sub>-0.000052</sub>	83.9800 <sup>+0.0055</sup> <sub>-0.0059</sub>	7.9907 <sup>+0.0042</sup> <sub>-0.0046</sub>	0.127592 <sup>+0.000029</sup> <sub>-0.000043</sub>	
478	5138.588677 <sup>+0.000048</sup> <sub>-0.000047</sub>	83.9806 <sup>+0.0055</sup> <sub>-0.0060</sub>	7.9928 <sup>+0.0040</sup> <sub>-0.0049</sub>	0.127603 <sup>+0.000035</sup> <sub>-0.000035</sub>	
479	5141.059254 <sup>+0.000044</sup> <sub>-0.000049</sub>	83.9840 <sup>+0.0060</sup> <sub>-0.0050</sub>	7.9905 <sup>+0.0041</sup> <sub>-0.0043</sub>	0.127588 <sup>+0.000038</sup> <sub>-0.000031</sub>	
480	5143.529887 <sup>+0.000045</sup> <sub>-0.000043</sub>	83.9797 <sup>+0.0061</sup> <sub>-0.0049</sub>	7.9888 <sup>+0.0043</sup> <sub>-0.0041</sub>	0.127577 <sup>+0.000036</sup> <sub>-0.000034</sub>	
481	5146.000644 <sup>+0.000042</sup> <sub>-0.000046</sub>	83.9659 <sup>+0.0053</sup> <sub>-0.0059</sub>	7.9895 <sup>+0.0038</sup> <sub>-0.0047</sub>	0.127580 <sup>+0.000033</sup> <sub>-0.000036</sub>	
482	5148.471133 <sup>+0.000046</sup> <sub>-0.000046</sub>	83.9813 <sup>+0.0052</sup> <sub>-0.0057</sub>	7.9898 <sup>+0.0043</sup> <sub>-0.0043</sub>	0.127584 <sup>+0.000036</sup> <sub>-0.000033</sub>	
483	5150.941691 <sup>+0.000043</sup> <sub>-0.000047</sub>	83.9799 <sup>+0.0054</sup> <sub>-0.0055</sub>	7.9899 <sup>+0.0042</sup> <sub>-0.0039</sub>	0.127591 <sup>+0.000034</sup> <sub>-0.000037</sub>	
484	5153.412285 <sup>+0.000044</sup> <sub>-0.000045</sub>	83.9755 <sup>+0.0049</sup> <sub>-0.0062</sub>	7.9902 <sup>+0.0040</sup> <sub>-0.0042</sub>	0.127583 <sup>+0.000035</sup> <sub>-0.000036</sub>	
486	5158.353590 <sup>+0.000045</sup> <sub>-0.000049</sub>	83.9865 <sup>+0.0057</sup> <sub>-0.0053</sub>	7.9909 <sup>+0.0043</sup> <sub>-0.0040</sub>	0.127592 <sup>+0.000034</sup> <sub>-0.000034</sub>	
487	5160.824096 <sup>+0.000046</sup> <sub>-0.000043</sub>	83.9753 <sup>+0.0054</sup> <sub>-0.0062</sub>	7.9909 <sup>+0.0047</sup> <sub>-0.0040</sub>	0.127592 <sup>+0.000035</sup> <sub>-0.000035</sub>	
488	5163.294713 <sup>+0.000041</sup> <sub>-0.000051</sub>	83.9746 <sup>+0.0056</sup> <sub>-0.0054</sub>	7.9907 <sup>+0.0042</sup> <sub>-0.0042</sub>	0.127587 <sup>+0.000032</sup> <sub>-0.000037</sub>	
489	5165.765446 <sup>+0.000051</sup> <sub>-0.000044</sub>	83.9836 <sup>+0.0058</sup> <sub>-0.0053</sub>	7.9897 <sup>+0.0047</sup> <sub>-0.0036</sub>	0.127587 <sup>+0.000032</sup> <sub>-0.000035</sub>	
490	5168.236001 <sup>+0.000042</sup> <sub>-0.000047</sub>	83.9756 <sup>+0.0056</sup> <sub>-0.0058</sub>	7.9913 <sup>+0.0041</sup> <sub>-0.0045</sub>	0.127593 <sup>+0.000031</sup> <sub>-0.000036</sub>	
491	5170.706625 <sup>+0.000045</sup> <sub>-0.000043</sub>	83.9790 <sup>+0.0048</sup> <sub>-0.0061</sub>	7.9905 <sup>+0.0046</sup> <sub>-0.0038</sub>	0.127590 <sup>+0.000036</sup> <sub>-0.000032</sub>	
492	5173.177189 <sup>+0.000049</sup> <sub>-0.000043</sub>	83.9814 <sup>+0.0057</sup> <sub>-0.0052</sub>	7.9907 <sup>+0.0039</sup> <sub>-0.0044</sub>	0.127598 <sup>+0.000034</sup> <sub>-0.000035</sub>	
493	5175.647822 <sup>+0.000043</sup> <sub>-0.000051</sub>	83.9678 <sup>+0.0050</sup> <sub>-0.0059</sub>	7.9901 <sup>+0.0042</sup> <sub>-0.0039</sub>	0.127581 <sup>+0.000033</sup> <sub>-0.000036</sub>	
494	5178.118439 <sup>+0.000039</sup> <sub>-0.000048</sub>	83.9781 <sup>+0.0060</sup> <sub>-0.0055</sub>	7.9907 <sup>+0.0048</sup> <sub>-0.0043</sub>	0.127598 <sup>+0.000034</sup> <sub>-0.000036</sub>	
495	5180.589204 <sup>+0.000040</sup> <sub>-0.000053</sub>	83.9747 <sup>+0.0048</sup> <sub>-0.0057</sub>	7.9892 <sup>+0.0043</sup> <sub>-0.0037</sub>	0.127582 <sup>+0.000035</sup> <sub>-0.000036</sub>	